Published in final edited form as:
Dev Cell. 2008 April ; 14(4): 523–534. doi:10.1016/j.devcel.2008.02.016.

Golgi localization of glycosyltransferases requires a Vps74p oligomer

Karl R. Schmitz[1,3,5], **Jingxuan Liu**[2,4,5], **Shiqing Li**[1], **Thanuja Gangi Setty**[1], **Christopher S. Wood**[2], **Christopher G. Burd**[2,*], and **Kathryn M. Ferguson**[1,*]

[1] Department of Physiology, University of Pennsylvania School of Medicine, Philadelphia, PA 19104, USA

[2] Department of Cell and Developmental Biology, University of Pennsylvania School of Medicine, Philadelphia, PA 19104, USA

[3] Graduate Group in Biochemistry and Molecular Biophysics, University of Pennsylvania School of Medicine, Philadelphia, PA 19104, USA

[4] Graduate Group in Cell and Molecular Biology, University of Pennsylvania School of Medicine, Philadelphia, PA 19104, USA

SUMMARY

The mechanism of glycosyltransferase localization to the Golgi apparatus is a longstanding question in secretory cell biology. All Golgi glycosyltransferases are type II membrane proteins with small cytosolic domains that contribute to Golgi localization. To date, no protein has been identified that recognizes the cytosolic domains of Golgi enzymes and contributes to their localization. Here we report that yeast Vps74p directly binds to the cytosolic domains of *cis* and *medial* Golgi mannosyltransferases and that loss of this interaction correlates with loss of Golgi localization of these enzymes. We have solved the X-ray crystal structure of Vps74p and find that it forms a tetramer, which we also observe in solution. Deletion of a critical structural motif disrupts tetramer formation, and results in loss of Vps74p localization and function. Vps74p is highly homologous to the human GMx33 Golgi matrix proteins, suggesting a conserved function for these proteins in the Golgi enzyme localization machinery.

INTRODUCTION

The Golgi apparatus has two primary functions: elaboration of glycoprotein and glycolipid carbohydrate chains, and the sorting of macromolecules to other organelles. Glycosylation of newly synthesized proteins is initiated in the ER and the carbohydrate chains are elaborated in the Golgi apparatus by sequentially-acting glycosyltransferases that are localized to successive compartments of the Golgi (Dean, 1999; Helenius and Aebi, 2004). Golgi *cis*, *medial*, and *trans* cisternae contain different complements of enzymes that generally reflect the order in which the enzymes function. This architecture is an essential feature of the Golgi apparatus,

*Address correspondence to either author: Kathryn M. Ferguson, Dept. Physiology, University of Pennsylvania School of Medicine, B400 Richards Building, 3700 Hamilton Walk, Philadelphia, PA 19104-6085, Phone: (215) 573-1207, E-mail: E-mail: ferguso2@mail.med.upenn.edu. Christopher G. Burd, Dept. Cell and Developmental Biology, University of Pennsylvania School of Medicine, BRB II/III, Room 1010, 421 Curie Blvd., Philadelphia, PA 19104-6058, Phone: (215) 573-5158, E-mail: E-mail: cburd@mail.med.upenn.edu.
[5]These authors contributed equally to this work

and elucidation of the mechanisms underlying glycosyltransferase compartmentalization is a major question in secretory cell biology (Pfeffer, 2007; Puthenveedu and Linstedt, 2005; Rabouille and Klumperman, 2005). Defects in the functions and localization of glycosyltransferases impact many aspects of human physiology, as exemplified by the varied and pleiotropic manifestations of congenital disorders of glycosylation (CDG) diseases (Jaeken and Matthijs, 2007).

Golgi glycosyltransferases are type II membrane proteins that contain a short (less than 25 amino acids) N-terminal cytosolic region, a single membrane-spanning segment, and a luminal domain consisting of a stalk region and catalytic domain. In general, robust localization of Golgi enzymes relies on contributions from each of these domains, although the membrane spanning and luminal domains appear to be most important (Colley, 1997; Machamer, 1993; Munro, 1998; Opat et al., 2001b). As the understanding of the molecular basis of Golgi enzyme localization has developed, it has become apparent that localization is defined dynamically with Golgi enzymes moving with anterograde cargo through the Golgi and being retrieved from distal compartments back to their resident compartment (Opat et al., 2001a; Puthenveedu and Linstedt, 2005). Coatomer (COP I) vesicles likely provide the predominant route for vesicle-mediated transport of Golgi enzymes within the Golgi (Puthenveedu and Linstedt, 2005; Rabouille and Klumperman, 2005). However, the cytosolic portions of the Golgi glycosyltransferases do not contain recognized COP I sorting signals so it is unclear how they are recognized by the retrieval system.

Several years ago we, and our colleagues carried out a genetic screen designed to identify genes that are essential in the absence of Ypt6p, a Rab GTPase that regulates intra-Golgi and endosome-to-Golgi trafficking (Tong et al., 2004). One of the genes identified in this screen was *VPS74*, which encodes a protein that is homologous to two human peripheral membrane proteins, GMx33α and GMx33β. These human proteins have been described as components of the Golgi matrix (Snyder et al., 2006; Wu et al., 2000), the fibrous assembly of cytosolic proteins associated with Golgi membranes (Slusarewicz et al., 1994). The Golgi matrix is proposed to provide a dynamic scaffold that couples cargo sorting and membrane transport with structural aspects of the organelle (Mogelsvang and Howell, 2006; Shorter and Warren, 2002). The high degree of conservation of Vps74p/GMx33 amino acid sequences in evolutionarily divergent organisms suggests that they have important functions at the Golgi apparatus, although very little is known about their structures and functions.

Here we describe functional and structural studies of yeast Vps74p. We find that Vps74p is required for the proper localization of a subset of Golgi enzymes, and that Vps74p interacts directly with the cytosolic domains of these enzymes. The X-ray crystal structure, to 2.8Å resolution, shows that Vps74p adopts a novel α-helical tetramer. This tetramer is also observed in solution and we find that this tetramer is functionally significant. Deletion of a β-hairpin in Vps74p that forms critical interactions in the crystallographically observed tetramer abrogates Vps74p oligomerization and disrupts its localization and function.

RESULTS

Vps74p is required for proper N- and O-linked protein glycosylation

The cell wall of budding yeast, *Saccharomyces cerevisiae*, is composed of a cross-linked mesh of glucan surrounded by an outer mannose-rich layer containing proteins decorated with up to 200 mannose residues (Lesage and Bussey, 2006). These “mannoproteins” also contain large amounts of mannose phosphate, conferring a net negative charge to the cell wall that is important for hydration and nutrient acquisition (Dean, 1999). Mutant yeast cells lacking the *VPS74* gene (*vps74*Δ) are deficient in the binding of Alcian Blue, a cationic dye that binds

negatively-charged polysaccharides, suggesting that Vps74p is required for incorporation of α-1,2-linked mannosephosphate into cell wall mannoproteins (Corbacho et al., 2005).

Defects in mannose phosphate incorporation into the cell wall could arise from failure at any of numerous biosynthetic steps. In a series of experiments, we establish that Vps74p is required for proper mannosylation of proteins. First, in standard pulse-chase assays we found that ^{35}S-labeled secreted proteins produced by *vps74*Δ cells have a higher electrophoretic mobility in than proteins produced by wild-type cells (Fig. 1A) – although the number of proteins and their relative abundances are similar. The mobility of invertase, an extensively N-glycosylated secreted protein, was also faster when immunoprecipitated from the media of *vps74*Δ cells than wild-type cells (Fig. 1B). Treatment with N-glycosidase F to remove N-linked carbohydrate chains digests both species of invertase to a protein with the same mobility (Fig. 1B). Therefore, the higher mobility of untreated invertase from *vps74*Δ cells is a consequence of reduced N-linked glycosylation. Similarly, mature vacuolar carboxypeptidase Y (mCPY) produced by *vps74*Δ cells migrates slightly faster than mCPY produced by wild-type cells (Fig. 1C), whereas the p1 form of CPY (which contains the unprocessed core oligosaccharide added in the endoplasmic reticulum) is unaffected. Since intracellular glycoproteins such as CPY receive only short, core-type N-linked sugars, these results suggest that *vps74*Δ cells have defects in Golgi processing of at least N-linked glycoproteins.

We next asked whether loss of any of several Golgi mannosyltransferases (Dean, 1999) phenocopies *vps74*Δ cells. As shown in Fig. 1A, the mobility profile of secreted proteins appears normal in cells with deletions of the *MNN1*, *MNN2*, *MNN5*, *MNN6*, or *MNN9* genes. By contrast the *kre2*Δ strain shows a similar, although not identical, profile to the *vps74*Δ strain. *KRE2* encodes an α-1,2-mannosyltransferase of the *medial* Golgi that functions in both N- and O-linked mannosylation (Lussier et al., 1997), leading us to ask whether Vps74p might play a role in O-linked carbohydrate modification in addition to the effect on processing of N-linked sugars shown above. To assess this, we analyzed processing of Hsp150p, an extensively O-glycosylated secreted protein whose expression is induced by heat shock (Russo et al., 1992). In wild-type cells, HA-tagged Hsp150p runs as a single band of approximately 150 kDa (Fig. 1D). In the *vps74*Δ mutant, multiple shorter species are also observed, and the largest most abundant species migrates below 150 kDa (Fig. 1D). These data indicate that Vps74p is required for proper mannosylation of O-linked as well as N-linked mannoproteins.

Vps74p is required for steady state localization of a subset of Golgi proteins

N-terminally GFP-tagged Vps74p (GFP-Vps74p) localizes to the Golgi apparatus as judged by its co-localization with Arf1p-mCherry, Cop1p-mCherry, and Sec7p-mCherry (Fig. S1). The most extensive co-localization is seen with Arf1p and Cop1p, components of the coatomer (COP I) vesicle coat. It is clear that Vps74p does not co-localize completely with any of the Golgi markers, suggesting that its localization is skewed towards (but not restricted to) early Golgi compartments. A substantial amount of GFP-Vps74p is also seen in the cytosol, but it does not co-localize detectably with Vps17p, a component of the retromer complex that is localized to endosomes.

Since Vps74p exists on the cytosolic side, and protein glycosylation occurs on the luminal side of secretory organelles, the role that Vps74p plays in glycosylation must be indirect. For example, it might influence the organization and/or composition of Golgi components. To test this hypothesis, we examined the localization of 12 different Golgi proteins, focusing first on enzymes of the N- and O-linked glycosylation pathways. Golgi proteins were tagged on their C-termini with GFP (using a 17 amino acid intervening linker) and expressed from their native loci in wild-type and *vps74*Δ cells (Fig. 2). In wild-type cells expressing Kre2p-GFP, Mnn2p-GFP, Mnn5p-GFP or Och1p-GFP, a Golgi-like punctate pattern was observed, consistent with the established *cis* and *medial* Golgi localization of these enzymes. By contrast, the localization

of each GFP-fusion protein was strikingly different in the *vps74*Δ strain. The GFP reporters localize to the lumen of the lysosome-like vacuole in addition to faint puncta resembling Golgi or endosomal compartments (Fig. 2). Since Golgi targeting of Kre2p is known to require contributions from the N-terminal cytosolic domain, as well as the membrane-spanning and stalk domains (amino acids 1-118) (Lussier et al., 1995), we constructed Kre2p(1-118)-GFP and find that it localizes almost exclusively to the Golgi of wild-type cells but to the vacuolar lumen in *vps74*Δ cells (Fig. 2). Loss of Golgi localization of these mannosyltransferases is not due to defective glycosylation. Localization of Kre2p-GFP, Mnn2p-GFP, Mnn5p-GFP, and Och1p-GFP is unaffected by deletion of *PMR1*, which encodes a Golgi calcium and manganese transporter required for glycosyltransferase activity (data not shown).

Not all Golgi proteins examined were mislocalized in *vps74*Δ cells (Fig. 2 and data not shown). Localization of the multi-membrane spanning Golgi proteins GFP-Rer1p, Sys1p-GFP, and Tvp15p-GFP, and of the TGN proteins Kex2p-GFP and GFP-Ste13p are unaffected by deletion of *VPS74*. Similarly, localization of several peripheral Golgi membrane proteins (Arf1p, Cop1p and Sec7p) and of Alg5p-GFP, an ER-localized glycosyltransferase, are unaffected by *VPS74* deletion. These results implicate Vps74p in specific retention of mannosyltransferases that reside in *cis* and *medial* Golgi compartments.

Vps74p binds the cytosolic domains of Golgi enzymes

To test the hypothesis that Vps74p interacts directly with Golgi mannosyltransferases through their N-terminal cytosolic domains, we generated fusion proteins with the first 15 amino acids of several different mannosyltransferases linked to the N-terminus of glutathione S-transferase (GST), thus leaving their N-termini free as in the native Golgi proteins. A similar GST fusion protein containing the 19 amino acid cytosolic portion of the type II vacuolar protein carboxypeptidase S (Cps1p) was included as a control. Varying proportions of GST fusion proteins and GST alone (with total bait protein held constant) were immobilized on glutathione-agarose beads and incubated with N-terminally epitope-tagged Vps74p, either as purified protein or supplied in *E.coli* lysates. Following five washes, bound proteins were eluted, analyzed by SDS-PAGE and visualized by immunoblotting (Fig. 3). Vps74p binds strongly to the Kre2p fusion protein and significantly to a number of the other fusion proteins. In each case, the amount of bound Vps74p tracked with the proportion of GST fusion protein added to the beads. By contrast, no binding was observed for GST alone, and association with Cps1p-GST was minimal.

Crystal structure of Vps74p at 2.8Å resolution

To better understand the protein at the molecular level, we solved the crystal structure of Vps74p. Full length *S. cerevisiae* Vps74p was expressed in *E. coli* and purified to homogeneity. Optimal crystals of native and selenomethionine-containing Vps74p that diffracted to a resolution of 2.8 Å were grown using polyethylene glycol (PEG) reservoir solutions containing 50 mM $CaCl_2$ and 10 mM EGTA. The crystal structure was determined by multi-wavelength anomalous dispersion (MAD) methods. Clear electron density for the protein was observed in experimentally phased maps, with the exception of the first 61 amino acids. MALDI (matrix-assisted laser desorption ionization) mass spectrometry of purified Vps74p provided no evidence of proteolysis of these amino acids, suggesting that the N-terminal region is intact but disordered in the crystal. It has been reported that deletion of the first 53 amino acids of GMx33 does not affect its Golgi targeting (Snyder et al., 2006; Wu et al., 2000), suggesting that this region of the protein may not be critical for at least this aspect of the protein's function. A variant lacking the first 59 amino acids of Vps74p (Vps74pΔ59) crystallized under similar conditions, in the same crystal form, and with the same arrangement of protein in the asymmetric unit (Table 1).

Vps74p forms a single globular domain that is predominantly α-helical (Fig. 4). A central four-helix bundle (α1, α2, α8, and α12) lies at the core of the protein. This core is surrounded by solvent-exposed loops and eight amphipathic helices that lie roughly orthogonal to the core bundle. An additional feature is formed by strands β3 and β4, which project as a β-hairpin away from the bulk of the helical domain, exposing hydrophobic residues at the side and tip. It seems unlikely that this conformation of the β-hairpin is stable independently in solution. Indeed, as discussed in detail below, this region is involved in an intermolecular interaction with a non-crystallographically related Vps74p molecule in the asymmetric unit.

The overall structure of Vps74p appears to be novel, bearing no strong homology to known protein folds as assessed by the DALI server (Holm et al., 1992), automated comparison against the CATH structural database (Pearl et al., 2005), and SSM comparison against the SCOP database (Murzin et al., 1995). DALI searches and sequence-based threading algorithms (Bennett-Lovsey et al., 2007) do highlight similarity between the β-hairpin region of Vps74p (α1, β3, β5, and α6) and the β-hairpin "wing" seen in winged helix proteins (Aravind et al., 2005; Gajiwala and Burley, 2000). As highlighted in green in Fig. 4D, both structures contain a β-hairpin projection on a helical base. Though most winged helix (WH) domains are found in DNA-binding proteins, the fold also occurs in protein-protein interfaces (Aravind et al., 2005). Most interestingly, the ESCRT-II proteins Vps22p, Vps25p and Vps36p all contain two repeats of a WH motif (Hierro et al., 2004; Teo et al., 2004). Vps22p and Vps36p both use their C-terminal WH motifs to interact with Vps25p. We suggest that the Vps74p WH-like region might also play an important role in protein-protein interactions (see below). The Vps74p β-hairpin region differs from WH motifs in its topology. Helices α1 and α6 replace H1 and H3 in the WH motif (H2 is missing). In both cases, the hairpin extends from the C-terminus of the last helix (α6 and H3).

Intriguingly, the WH-like motif of Vps74p contributes to intermolecular interactions in the tetramer seen in crystals. Vps74p crystallized with 4 molecules in the asymmetric unit, producing a tetramer with two-fold, non-crystallographic symmetry. To assess whether this tetramer might be significant, we analyzed the oligomeric state of Vps74p in solution. In solutions containing 10 mM $CaCl_2$ plus 10 mM EGTA, clear evidence of tetramer formation was observed in analytical ultracentrifugation studies (Fig. 5A). Based on the distribution of Vps74p into monomer and tetramer populations, we estimate a dissociation constant (K_D) for the monomer-tetramer equilibrium in the range of 5–10 μM. The formation of some higher order species (not shown) prevented a more quantitative analysis of the stability of the tetramer. By contrast, without $CaCl_2$ and EGTA (in 25 mM HEPES, 150 mM NaCl, pH 7.5), Vps74p appears monomeric in analytical ultracentrifugation (Fig. 5A), size exclusion chromatography (SEC), and dynamic light scattering (data not shown) experiments. Only at high protein concentrations (> 25 μM) could higher-order species be detected under these conditions, and data were consistent only with weak dimerization (K_D > 100 μM). We do not have an explanation for the effect of Ca/EGTA on Vps74p tetramerization. No strong electron density attributable to bound calcium or EGTA was evident in the structure, although the presence of such sites cannot be ruled out on the basis of these data alone. The fact that tetramers are observed both in crystals and in certain solution conditions suggests that the protein contacts observed in the crystal can occur in solution and may be functionally significant. Indeed, in support of this, we find that addition of Ca/EGTA to the buffer in the GST-binding assay leads to a modest (approximately 2-fold) enhancement in binding of Vps74p to Kre2p-GST (Fig. 5B).

As shown in Figs. 5C & D, the Vps74p tetramer comprises two central (yellow and cyan) and two peripheral (red and blue) subunits, stabilized by three distinct types of interaction that we refer to as the "inner" (Fig. 5C), "β-hairpin" (Fig. 5D), and "outer" (Fig. 5D) interactions. The inner interaction involves a symmetric association of the two central Vps74p molecules through

an interface consisting of their α1-α2 and α9-α10 loops (Fig. 6A & B). This interface has the largest associated buried surface area of the three interaction types (burying 1255 $Å^2$ on each molecule), and is stabilized primarily through electrostatic and hydrogen-bonds (Table S1). The β-hairpin interaction links a peripheral molecule (e.g. the red molecule in Fig. 5C,D) to one of its two central interaction partners (yellow in Fig. 5C,D). This interaction involves the mutual burial of hydrophobic side chains by the β3/β4 hairpins of two Vps74p molecules (Fig. 6C), and the projection of an FFLF motif at the tip of each hairpin (residues 201–204) into a pocket formed by α6 and the α1-α2 loop on the partner (Fig. 6C). This projection of hydrophobic side chains from the tip of the β-hairpin into a pocket of a binding partner is a feature observed in WH motif-driven protein-protein interactions (Haering et al., 2004; Hierro et al., 2004; Teo et al., 2004), including those that stabilize the ESCRT-II complex (Fig. 4E). The β-hairpin interaction buries ~1000 $Å^2$ on each subunit, of which an unusually high proportion (70%) is hydrophobic (Lo Conte et al., 1999). Finally, the outer interaction connects each peripheral molecule to its other central interaction partner (cyan Fig. 5D & 6A). This is an asymmetric interaction in which amino acids from the α1-α2 and α9-α10 loops of the peripheral subunit contact the β2-α3 and α5-α6 regions of the central subunit. Although this outer interaction buries the smallest area (~750 $Å^2$ per molecule), the simultaneous binding of each peripheral subunit to two central subunits is likely to be critical for stabilizing the tetrameric assembly. It is notable that the C-termini of the central subunits are relatively occluded in the tetramer, by both an outer and a β-hairpin interaction (Fig. 6A). A bulky group (such as GFP) fused to the Vps74p C-terminus (Vps74p-GFP) would be expected to hinder tetramerization. This may account for the observed mislocalization (Huh et al., 2003) and loss of *in vivo* function (Fig. 7A) of Vps74p-GFP.

The β-hairpin appears to play a key role in formation of the crystallographically-observed Vps74p tetramer. Its disruption would be predicted to prevent tetramerization, while leaving the central dimer intact. To test this, we generated a variant of Vps74p lacking the β3/β4 hairpin, Vps74pΔ (197–208). In the Ca/EGTA buffer that promotes tetramer assembly in full-length Vps74p, Vps74pΔ (197–208) was found to sediment only as a distribution of monomers and dimers, with no evidence of tetramer (Fig. 5A). These data demonstrate that the β-hairpin is required for tetramer, but not dimer, formation.

In addition to the substantial buried surface areas and shape complementarities (Table S1) of the protein-protein interfaces in the Vps74p tetramer, the degree of sequence conservation suggests that the tetramer is physiologically significant. The regions of Vps74p that form the interaction surfaces in the tetramer, including the β3/β4 hairpin, are strongly conserved across fungal and animal homologs (Fig. S2). Further, by examining the degree of conservation of solvent-exposed residues on the surface of the tetramer, distinct regions are apparent (Fig. 6D). The lower concave surface (bottom view) possesses a high degree of sequence conservation, while the upper convex surface (top view) does not. This polarization of conserved surface-exposed amino acids is mirrored in the electrostatic potential of the tetramer (Fig. 6E), which may be relevant since the N-terminal tails of mannosyltransferases have substantial basic character. The conserved concave face of Vps74p is negatively-charged whereas the less conserved convex surface is more basic. Additional regions of high amino acid conservation, appreciated in the top view in Fig. 6D, also correlate with regions of strong negative electrostatic potential (Fig. 6E). In addition to supporting the relevance of the oligomer that we observe in the crystal, these observations may have implications for the function of Vps74p (see Discussion).

Oligomerization is required for Vps74p function

Our structural and biophysical analyses indicate that Vps74p forms dimers and tetramers in solution, with key contributions to tetramer formation from the β-hairpin. To determine

whether Vps74p function requires oligomerization, we asked whether Vps74pΔ (197–208) that lacks the β-hairpin, or another variant that lacks only the four hydrophobic amino acids at the β-hairpin tip (F201-F204: Fig. 6C) can functionally replace the wild-type protein. As shown in Fig. 7, expression of neither protein in *vps74*Δ cells rescues the glycosylation or Kre2p-GFP localization defects reported for these cells in Figs. 1A and 2. Importantly, *E. coli*-expressed forms of the two β-hairpin-disrupted Vps74p variants fail to bind the Kre2p-GST fusion protein (Fig. 7B). Either the β-hairpin is directly involved in the interaction of Vps74p with Kre2p-GST or Vps74p tetramerization (which requires the β-hairpin, Fig. 5A) is critical for this interaction. The increased binding of Vps74p to Kre2p-GST in the presence of Ca/EGTA buffer (Fig. 5B), which also promotes oligomerization in solution studies (Fig 5A), supports a role for Vps74p tetramerization. The binding of Vps74p to Kre2p-GST is enhanced by conditions that promote Vps74p tetramers, and abolished for altered Vps74p that cannot form tetramers.

Deletion of the β-hairpin abolishes Golgi localization of GFP-Vps74p (Fig. 7D). However these Vps74p variants do not induce any dominant negative effects in yeast. Using the secreted protein pulse-chase assay, we find that neither Vps74pΔ (197–208) nor Vps74pΔ (201–204), expressed from multi-copy 2μ vectors, affects the electrophoretic mobility of ^{35}S-labeled secreted proteins in wild type cells (data not shown). Finally, since the amino acid sequence of Vps74p in the β-hairpin region is highly homologous to that of human GMx33α and GMx33β (Fig. S2), we asked whether analogous mutations also affect targeting of GMx33α in human cells. As shown in Fig. 7E, deletion of the β-hairpin (190–201) from GMx33α reduces its Golgi localization in HeLa cells.

DISCUSSION

It has been postulated for many years that components of the Golgi matrix bind directly to the cytosolic domains of Golgi enzymes, thereby immobilizing them in their resident cisternae (Nilsson et al., 1994; Nilsson et al., 1993; Slusarewicz et al., 1994). We provide evidence for interaction of Vps74p with the cytosolic aspect of certain Golgi mannosyltransferases, and correlate this with their Golgi retention. Vps74p forms tetramers in crystals and in solution, mediated by interactions reminiscent of those that stabilize the ESCRT II complex. Deletions in a key β-hairpin disrupt Vps74p oligomerization in solution, and abolish Vps74p function and subcellular localization. These observations suggest that tetramerization is functionally important for Vps74p. A striking feature of the tetramer is a cavity that is 70Å wide and 30Å deep, the surface of which is acidic, and is lined by highly-conserved amino acids (Fig. 6D & E). The conservation suggests that this is a functionally important surface. However, it seems unlikely to represent a binding site for the short (8–20 amino acids) N-terminal tails of yeast Golgi mannosyltransferases, since it is too large and deep to provide a complementary recognition surface for these short epitopes. Rather, the size and strong surface conservation of this cavity suggest that it may be a binding site for a similarly well-conserved, but as yet unidentified, larger protein ligand. Other conserved regions with negative charge occur outside this large cavity, and are more prominent on the Vps74p tetramer than on the monomer (Fig. 6). We suggest that these regions are candidate interaction sites for the mannosyltransferase cytosolic domains, which carry a positive charge. Additional studies are required to further elucidate the molecular details of the interaction of Vps74p with these Golgi enzymes.

Snyder *et al.* have shown that the association of human GMx33 with Golgi membranes *in vivo* is dynamic (Snyder et al., 2006) and this is likely also the case for Vps74p. At steady state, a substantial fraction of Vps74p is cytosolic (Fig. 7D and S1). Since tetramerization appears to be required for Golgi localization of Vps74p, and is relatively weak, it is possible that the cytosolic pool of wild-type Vps74p represents a monomeric population *in vivo*. Vps74p may exist in a regulated dynamic equilibrium between cytosolic monomers and Golgi-associated oligomers *in vivo*, and this might be intimately linked to its function. The structure suggests

that conformational changes in Vps74p are likely to accompany tetramer dissociation. Simple exposure of the β-hairpin would require energetically costly solvation of its largely hydrophobic surface. Moreover, no potentially stabilizing intramolecular interactions can be seen between the hairpin and its associated helical core. One possibility is that the β-hairpin of monomeric Vps74p makes intramolecular interactions with the α1-α2 loop. Fig. 4D indicates that this would require only a small conformational change, and the result would resemble the interaction seen between the β-hairpin and the H1/H2 loop region frequently seen in WH motifs (Fig 4D). The apparent flexibility of the α1-α2 loop evident in the crystal structure is consistent with this hypothesis. The α1-α2 loop occupies distinct conformations in the central and peripheral subunits of the tetramer, due to its participation in inner and outer interactions, respectively. A conformational change in the region of the β-hairpin and the α1-α2 loop might offer a means for regulating function. GMx33 is phosphorylated (Wu et al., 2000) and one well-conserved potential phosphorylation site occurs at S86 in the α1-α2 loop.

The hypothesis that emerges from our studies is that a cycle of Vps74p self-association and dissociation may contribute to the dynamic recruitment of Vps74p to Golgi enzymes and possibly to other proteins associated with Golgi membranes. Although the mechanisms by which Golgi enzymes are localized to and within the Golgi apparatus are matters of considerable debate, it is clear that multiple mechanisms acting in concert underlie dynamic localization of Golgi enzymes. Vps74p might function in the Golgi enzyme retrieval system, the principal structural components of which are COP I vesicles, the conserved oligomeric Golgi (COG) complex, and SNARE proteins. Glick and colleagues have pointed out that steady state localization of *cis* and *medial* Golgi proteins can arise from their preferential incorporation into COP I vesicles that bud from distal cisternae (Glick et al., 1997). Since Golgi enzymes and most Golgi SNARE proteins do not contain known COP I sorting signals in their cytosolic domains, Vps74p could facilitate sorting of these proteins into COP I vesicles. In preliminary experiments we have not detected binding of Vps74p to COP I subunits or to Arf1p, but we have found that mutations in COP I subunits (*sec21-1* and *sec27-1*) result in partial mislocalization of Kre2p to the vacuole, akin to the phenotype of *vps74*Δ mutants (unpublished observations). In contrast, mutations in COG subunit genes result in an accumulation of Golgi enzymes in dispersed vesicles (Bruinsma et al., 2004; Zolov and Lupashin, 2005), suggesting that Vps74p functions at or before the packaging of Golgi enzymes into COP I vesicles. Identification and full characterization of Vps74p binding partners will be key to more precisely defining the function of Vps74p at the Golgi.

EXPERIMENTAL PROCEDURES

Yeast methods

Yeast strains were grown in standard media as required for selection of transformants and maintenance of plasmids. Yeast strains were constructed in the BY4742 background (*MAT*α *his3-1, leu2-0, met15-0, ura3-0)* by integration of gene-targeted PCR-generated DNAs (Longtine et al., 1998) to ensure expression from native gene promoters. N-terminal GFP-tagged Vps74p was expressed using the constitutive *PRC1* promoter in the pGO-GFP vector (Cowles et al., 1997). Altered forms of Vps74p, in pRS415, were expressed from the native *VPS74* promoter.

Molecular biology methods and reagents

Standard molecular biological protocols and reagents were used. The sequences of all PCR-generated DNAs were confirmed. Monoclonal antibodies included: anti-HA (1:1000 – Covance), anti-T7 (1:10,000 – Novagen), anti-GFP (1:1000 – Covance) and sheep anti-mouse HRP-conjugate (1:5000 - Amersham Biosciences).

Protein Expression and Purification

To generate Golgi protein-GST fusion proteins, PCR methods were used to introduce the first 15 codons of *KRE2*, *MNN2*, *MNN5*, and *OCH1* upstream of the GST open reading frame of pGEX-KG, and a stop codon before the multiple cloning site. Use of an NcoI cloning site altered codon 2 of *MNN2* and *MNN5* (Leu to Val), and of *OCH1* (Ser to Ala). Dr. David Katzmann (Mayo Research Foundation) provided the Cps1-GST fusion plasmid. The *VPS74* locus was amplified by PCR and cloned into pET-28a that encodes a T7 epitope tag at the N-terminus of the protein (T7-Vps74p) or into modified pET-21 containing a TEV-recognition cleavage site between the N-terminal hexa-histidine tag and the multiple cloning site (H_6-Vps74p). PCR methods were used to generate vectors to express altered forms of Vps74p.

GST fusion proteins and T7-Vps74p were expressed in *E. coli* BL21 (DE3) (Novagen) by induction with IPTG overnight at 22° C (GST fusions) or for three hours at 37°C (T7-Vps74p). Cell were lysed in PBS containing 1X Complete Mini protease inhibitor cocktail (Roche) using lysozyme and sonication. Clarified lysate was stored at −80° C. To produce pure Vps74p, H_6-Vps74p or T7-Vps74p were expressed in BL21-CodonPlus (DE3) RP *E. coli* (Stratagene) by induction with IPTG for 3 h at 37°C. Selenomethionine-derivitized protein (SeMet-Vsp74p) was expressed in B834 (DE3) *E. coli* (Novagen) in simplified minimal medium (Guerrero et al., 2001). Cells were lysed by sonication in 25 mM Na_2HPO_4/NaH_2PO_4, 250 mM NaCl, 10% glycerol, pH 8.0 and clarified lysates applied to a Ni-NTA (Qiagen) affinity column. TEV protease (150 μg/5 mg Vps74p) was added to eluted H_6-Vps74p and the proteins dialyzed overnight against 50 mM Tris, 50 mM NaCl, 1 mM DTT, pH 8.0. TEV-digested Vps74p or undigested T7-Vps74p were further purified by anion exchange chromatography (Source Q, GE Healthcare) and size exclusion chromatography (Superose 12, GE Healthcare). Purified protein was concentrated to 10 mg/ml and stored in 10 mM HEPES, 150 mM NaCl, 1 mM TCEP, pH 7.5.

Crystallographic methods

Crystals were grown by hanging-drop vapor diffusion. 10 mg/ml Vps74p or SeMet-Vsp74p was mixed with an equal volume of 8% PEG 3350, 5% ethylene glycol, 50 mM MES, 50 mM NaCl, 50 mM $CaCl_2$, 10 mM EGTA, pH 6.0 (crystallization buffer), and suspended over 300 μL crystallization buffer. Hexagonal crystals (75 × 75 × 300 μm) were cryo-stabilized by brief exposure to crystallization buffer supplemented with 15% ethylene glycol, and flash frozen in liquid nitrogen. Vps74pΔ59 crystals were generated similarly, but grown in 5% glycerol, 15% PEG 3350, 100 mM citrate, 0.75 M KCl, 50 mM EGTA, pH 6.0, and stabilized in this buffer containing 15% glycerol.

X-ray diffraction data were collected at CHESS F1 and APS ID-23 D beamlines. Data were processed with HKL-2000 (Otwinowski and Minor, 1997). The protein substructure was determined using data collected from the SeMet-Vps74p crystals, using MAD methods in the program SHELX C/D/E (Schneider and Sheldrick, 2002; Sheldrick, 2002). All but the first 61 amino acids of Vps74p could be traced in this experimentally phased map using the program Coot (Emsley and Cowtan, 2004). The structure was refined against data from native Vps74p and Vps74pΔ59 crystals using the programs Refmac (CCP4, 1994) and CNS (Brunger et al., 1998). Crystallographic statistics are in Table 1. The coordinates have been submitted to the PDB with ID's 2ZIH (Vps74p) and 2ZII (Vps74pΔ59).

Sedimentation velocity analysis

Sedimentation velocity analytical ultracentrifugation experiments were performed in a Beckman Optima XL-A instrument, at 40,000 or 50,000 rpm, at 20°C, and in 150 mM NaCl, 20 mM HEPES, pH 7.5, ± 10 mM EGTA/10 mM $CaCl_2$. Continuous distributions were calculated by *c(s)* analysis in SEDFIT (Schuck, 2000), using solution and protein property

estimates from SEDNTERP (http://www.jphilo.mailway.com/). Sedimentation coefficients for monomer, dimer, and tetramer were estimated with HYDROPRO (Garcia De La Torre et al., 2000).

In vitro protein binding assays

GST fusion proteins (~ 25 μg) were immobilized on Glutathione (GSH) Sepharose 4B (Amersham) by rocking for 1 hour at room temperature in 0.5ml PBS. The total amount of protein was kept constant but the ratio of GST fusion:GST was varied by mixing appropriate lysates prior to incubation with GSH beads. Beads were washed three times with 1 ml PBS and resuspended in 350 μl of binding buffer (PBS plus 5 mM $MgCl_2$, 0.1% Triton X-100). Purified T7-Vps74p, to yield a final concentration of 20 μM, or cell lysates containing T7-Vps74p (~ 30 μg) were added, the volume adjusted to 300 μl with binding buffer, and mixtures incubated at 4° C for 3 hours. Beads were washed (5 × 1 ml) with binding buffer, bound proteins eluted with 2X SDS sample buffer and analyzed by 10% SDS-PAGE. T7-Vps74p was detected by blotting with anti-T7 antibody and GST proteins by Coomassie blue staining.

Fluorescence microscopy

3-D image stacks were collected at 0.5 μm z-increments on an Applied Precision DeltaVision workstation based on an Olympus IX-70 inverted microscope, using a 60x NA 1.4 oil immersion lens. Images were deconvolved using the iterative-constrained algorithm (Agard, 1984) and the measured point spread function, and were scaled using ImageJ 1.38 (Rasband).

Supplementary Material

Refer to Web version on PubMed Central for supplementary material.

Acknowledgments

We thank David Katzmann for providing reagents, Todd Graham, James Shorter, Mark Lemmon and members of the Ferguson and Burd laboratories for critical comments on the manuscript. This work was supported by grants from the National Institutes of Health (GM61221 to CGB and CA112552 to KMF). KMF is also supported by a Career Award in the Biomedical Sciences from the Burroughs Wellcome Fund and is the Dennis and Marsha Dammerman Scholar supported by the Damon Runyon Cancer Research Foundation (DRS-52-06). KRS is supported in part by a Predoctoral Fellowship (BC051591) from the U.S. Army Breast Cancer Research Program. This work is based upon research conducted at (i) the Cornell High Energy Synchrotron Source (CHESS), which is supported by the NSF under award DMR 97-13424, using the Macromolecular Diffraction at CHESS (MacCHESS) facility, which is supported by award RR-01646 from the NIH, through its National Center for Research Resources and (ii) the GM/CA CAT at the Advanced Photon Source (APS) that has been funded in whole or in part with Federal funds from the National Cancer Institute (Y1-CO-1020) and National Institute of General Medical Science (Y1-GM-1104). Use of APS was supported by the U.S. Department of Energy, Basic Energy Sciences, Office of Science, under contract No. W-31-109-ENG-38.

References

Agard DA. Optical sectioning microscopy: cellular architecture in three dimensions. Annu Rev Biophys Bioeng 1984;13:191–219. [PubMed: 6742801]

Aravind L, Anantharaman V, Balaji S, Babu MM, Iyer LM. The many faces of the helix-turn-helix domain: transcription regulation and beyond. FEMS Microbiol Rev 2005;29:231–262. [PubMed: 15808743]

Baker NA, Sept D, Joseph S, Holst MJ, McCammon JA. Electrostatics of nanosystems: application to microtubules and the ribosome. Proc Natl Acad Sci USA 2001;98:10037–10041. [PubMed: 11517324]

Bennett-Lovsey RM, Herbert AD, Sternberg MJ, Kelley LA. Exploring the extremes of sequence/structure space with ensemble fold recognition in the program Phyre. Proteins. 2007

Brunger AT, Adams PD, Clore GM, DeLano WL, Gros P, Grosse-Kunstleve RW, Jiang JS, Kuszewski J, Nilges M, Pannu NS, et al. Crystallography & NMR system: A new software suite for macromolecular structure determination. Acta Crystallogr 1998;D54:905–921.

CCP4. The CCP4 Suite: Programs for Protein Crystallography. Acta Crystallogr 1994;D50:760–763.

Colley KJ. Golgi localization of glycosyltransferases: more questions than answers. Glycobiology 1997;7:1–13. [PubMed: 9061359]

Corbacho I, Olivero I, Hernandez LM. A genome-wide screen for Saccharomyces cerevisiae nonessential genes involved in mannosyl phosphate transfer to mannoprotein-linked oligosaccharides. Fungal Genet Biol 2005;42:773–790. [PubMed: 15993632]

Cowles CR, Odorizzi G, Payne GS, Emr SD. The AP-3 adaptor complex is essential for cargo-selective transport to the yeast vacuole. Cell 1997;91:109–118. [PubMed: 9335339]

Dean N. Asparagine-linked glycosylation in the yeast Golgi. Biochim Biophys Acta 1999;1426:309–322. [PubMed: 9878803]

DeLano, WL. The PyMOL Molecular Graphics System. Palo Alto, CA, USA: DeLano Scientific; 2004.

Emsley P, Cowtan K. Coot: model-building tools for molecular graphics. Acta Crystallogr 2004;D60:2126–2132.

Garcia De La Torre J, Huertas ML, Carrasco B. Calculation of hydrodynamic properties of globular proteins from their atomic-level structure. Biophys J 2000;78:719–730. [PubMed: 10653785]

Glick BS, Elstron T, Oster G. A cisternal maturation mechansim can explain the asymmetry of the Gogli stack. FEBS Lett 1997;414:177–181. [PubMed: 9315681]

Guerrero SA, Hecht HJ, Hofmann B, Biebl H, Singh M. Production of selenomethionine-labelled proteins using simplified culture conditions and generally applicable host/vector systems. Appl Microbiol Biotechnol 2001;56:718–723. [PubMed: 11601620]

Haering CH, Schoffnegger D, Nishino T, Helmhart W, Nasmyth K, Lowe J. Structure and stability of cohesin's Smc1-kleisin interaction. Mol Cell 2004;15:951–964. [PubMed: 15383284]

Helenius A, Aebi M. Roles of N-linked glycans in the endoplasmic reticulum. Annu Rev Biochem 2004;73:1019–1049. [PubMed: 15189166]

Hierro A, Sun J, Rusnak AS, Kim J, Prag G, Emr SD, Hurley JH. Structure of the ESCRT-II endosomal trafficking complex. Nature 2004;431:221–225. [PubMed: 15329733]

Holm L, Ouzounis C, Sander C, Tuparev G, Vriend G. A database of protein structure families with common folding motifs. Prot Sci 1992;1:1691–1698.

Huh WK, Falvo JV, Gerke LC, Carroll AS, Howson RW, Weissman JS, O'Shea EK. Global analysis of protein localization in budding yeast. Nature 2003;425:686–691. [PubMed: 14562095]

Jaeken J, Matthijs G. Congenital disorders of glycosylation: a rapidly expanding disease family. Annu Rev Genomics Hum Genet 2007;8:261–278. [PubMed: 17506657]

Lesage G, Bussey H. Cell wall assembly in Saccharomyces cerevisiae. Microbiol Mol Biol Rev 2006;70:317–343. [PubMed: 16760306]

Lo Conte L, Chothia C, Janin J. The atomic structure of protein-protein recognition sites. J Mol Biol 1999;285:2177–2198. [PubMed: 9925793]

Longtine MS, McKenzie A 3rd, Demarini DJ, Shah NG, Wach A, Brachat A, Philippsen P, Pringle JR. Additional modules for versatile and economical PCR-based gene deletion and modification in Saccharomyces cerevisiae. Yeast 1998;14:953–961. [PubMed: 9717241]

Lussier M, Sdicu AM, Bussereau F, Jacquet M, Bussey H. The Ktr1p, Ktr3p, and Kre2p/Mnt1p mannosyltransferases participate in the elaboration of yeast O- and N-linked carbohydrate chains. J Biol Chem 1997;272:15527–15531. [PubMed: 9182588]

Lussier M, Sdicu AM, Ketela T, Bussey H. Localization and targeting of the Saccharomyces cerevisiae Kre2p/Mnt1p alpha 1,2-mannosyltransferase to a medial-Golgi compartment. J Cell Biol 1995;131:913–927. [PubMed: 7490293]

Machamer CE. Targeting and retention of Golgi membrane proteins. Curr Opin Cell Biol 1993;5:606–612. [PubMed: 8257601]

Mogelsvang S, Howell KE. Global approaches to study Golgi function. Curr Opin Cell Biol 2006;18:438–443. [PubMed: 16781854]

Munro S. Localization of proteins to the Golgi apparatus. Trends Cell Biol 1998;8:11–15. [PubMed: 9695801]

Murzin AG, Brenner SE, Hubbard T, Chothia C. SCOP: a structural classification of proteins database for the investigation of sequences and structures. J Mol Biol 1995;247:536–540. [PubMed: 7723011]

Nilsson T, Hoe MH, Slusarewicz P, Rabouille C, Watson R, Hunte F, Watzele G, Berger EG, Warren G. Kin recognition between medial Golgi enzymes in HeLa cells. EMBO J 1994;13:562–574. [PubMed: 8313901]

Nilsson T, Slusarewicz P, Hoe MH, Warren G. Kin recognition. A model for the retention of Golgi enzymes. FEBS Lett 1993;330:1–4. [PubMed: 8370450]

Opat AS, Houghton F, Gleeson PA. Steady-state localization of a medial-Golgi glycosyltransferase involves transit through the trans-Golgi network. Biochem J 2001a;358:33–40. [PubMed: 11485549]

Opat AS, van Vliet C, Gleeson PA. Trafficking and localisation of resident Golgi glycosylation enzymes. Biochimie 2001b;83:763–773. [PubMed: 11530209]

Otwinowski, Z.; Minor, W. Processing of X-ray Diffraction Data Collected in Oscillation Mode. In: Carter, CW., Jr; Sweet, RM., editors. Macromolecular Crystallography. New York: Academic Press; 1997. p. 307-326.

Pearl F, Todd A, Sillitoe I, Dibley M, Redfern O, Lewis T, Bennett C, Marsden R, Grant A, Lee D, et al. The CATH Domain Structure Database and related resources Gene3D and DHS provide comprehensive domain family information for genome analysis. Nucleic Acids Res 2005;33:D247–251. [PubMed: 15608188]

Pfeffer SR. Unsolved mysteries in membrane traffic. Annu Rev Biochem 2007;76:629–645. [PubMed: 17263661]

Puthenveedu MA, Linstedt AD. Subcompartmentalizing the Golgi apparatus. Curr Opin Cell Biol 2005;17:369–375. [PubMed: 15975779]

Rabouille C, Klumperman J. Opinion: The maturing role of COPI vesicles in intra-Golgi transport. Nat Rev Mol Cell Biol 2005;6:812–817. [PubMed: 16167055]

Rasband, WS. ImageJ. U. S. National Institutes of Health; Bethesda, Maryland, USA : 1997–2007. http://rsb.info.nih.gov/ij/

Russo P, Kalkkinen N, Sareneva H, Paakkola J, Makarow M. A heat shock gene from Saccharomyces cerevisiae encoding a secretory glycoprotein. Proc Natl Acad Sci USA 1992;89:3671–3671. [PubMed: 1570286]

Schuck P. Size-distribution analysis of macromolecules by sedimentation velocity ultracentrifugation and lamm equation modeling. Biophys J 2000;78:1606–1619. [PubMed: 10692345]

Shorter J, Warren G. Golgi architecture and inheritance. Annu Rev Cell Dev Biol 2002;18:379–420. [PubMed: 12142281]

Slusarewicz P, Nilsson T, Hui N, Watson R, Warren G. Isolation of a matrix that binds medial Golgi enzymes. J Cell Biol 1994;124:405–413. [PubMed: 8106542]

Snyder CM, Mardones GA, Ladinsky MS, Howell KE. GMx33 associates with the trans-Golgi matrix in a dynamic manner and sorts within tubules exiting the Golgi. Mol Biol Cell 2006;17:511–524. [PubMed: 16236792]

Teo H, Perisic O, Gonzalez B, Williams RL. ESCRT-II, an endosome-associated complex required for protein sorting: crystal structure and interactions with ESCRT-III and membranes. Dev Cell 2004;7:559–569. [PubMed: 15469844]

Tong AH, Lesage G, Bader GD, Ding H, Xu H, Xin X, Young J, Berriz GF, Brost RL, Chang M, et al. Global mapping of the yeast genetic interaction network. Science 2004;303:808–813. [PubMed: 14764870]

Wu CC, Taylor RS, Lane DR, Ladinsky MS, Weisz JA, Howell KE. GMx33: a novel family of trans-Golgi proteins identified by proteomics. Traffic 2000;1:963–975. [PubMed: 11208086]

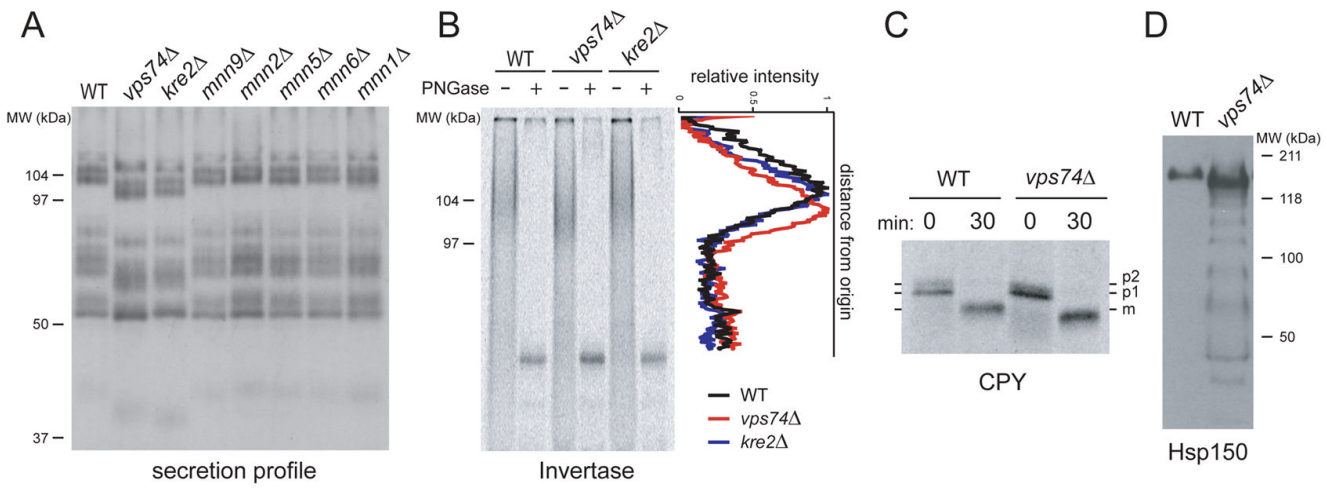

Figure 1. The yeast *vps74Δ* strain has defects in N- and O-linked glycosylation

(A) Pulse-chase secretion assay. The indicated strains were pulse-labeled with ^{35}S-methionine/cysteine (Met/Cys) for 15 minutes and chased with unlabelled Met/Cys for 45 minutes. Secreted proteins were precipitated from clarified media and visualized, after SDS-PAGE, by fluorography. WT = wild-type strain.

(B) Pulse-chase immunoprecipitation analysis of secreted invertase. The indicated strains, expressing a constitutively secreted invertase, were pulse-labeled with ^{35}S-Met/Cys for 30 minutes and chased with unlabelled Met/Cys for 30 minutes. Invertase was immunoprecipitated from clarified media using an anti-invertase antibody. Samples were divided and one fraction treated with PNGase F. After SDS-PAGE autoradiography, the untreated lanes were scanned using ImageJ. The relative intensities of the signals are plotted.

(C) Pulse-chase immunoprecipitation analysis of carboxypeptidase Y (CPY). Wild-type and *vps74Δ* strains were pulse-labeled with ^{35}S-Met/Cys for 10 minutes and chased with unlabelled Met/Cys for 30 minutes. CPY was immunoprecipitated from cultures and visualized by SDS-PAGE fluorography. The positions of the p1 ER-modified form, p2 Golgi-modified form, and vacuole localized mCPY in wild-type cells are indicated.

(D) Secretion of Hsp150. Wild-type and *vps74Δ* strains expressing HA epitope-tagged Hsp150p were incubated at 37°C for one hour. Proteins were precipitated from clarified media with TCA and analyzed using Western blots probed with anti-HA antibody. The migration of molecular mass standards (kDa) is indicated.

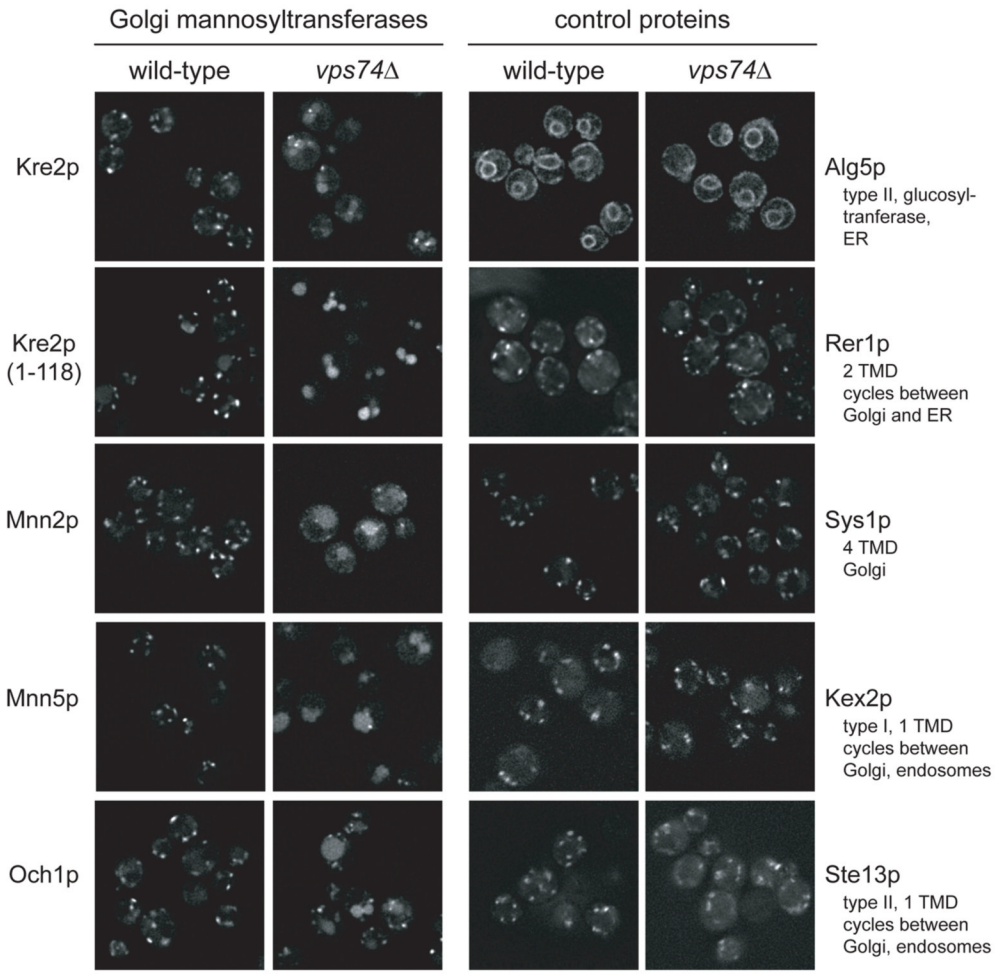

Figure 2. Golgi mannosyltransferases are mislocalized in *vps74*Δ, while other Golgi and ER proteins are not

Deconvolution fluorescence microscopy was used to visualize the indicated GFP-tagged proteins in wild-type and *vps74*Δ cells. Proteins were expressed from their native chromosomal loci with a C-terminal 17 amino acid linker followed by GFP, except Rer1p and Ste13p, which were expressed from single copy vectors with a N-terminal GFP driven by the *PRC1* promoter. One plane of the deconvolved Z-axis stack is shown.

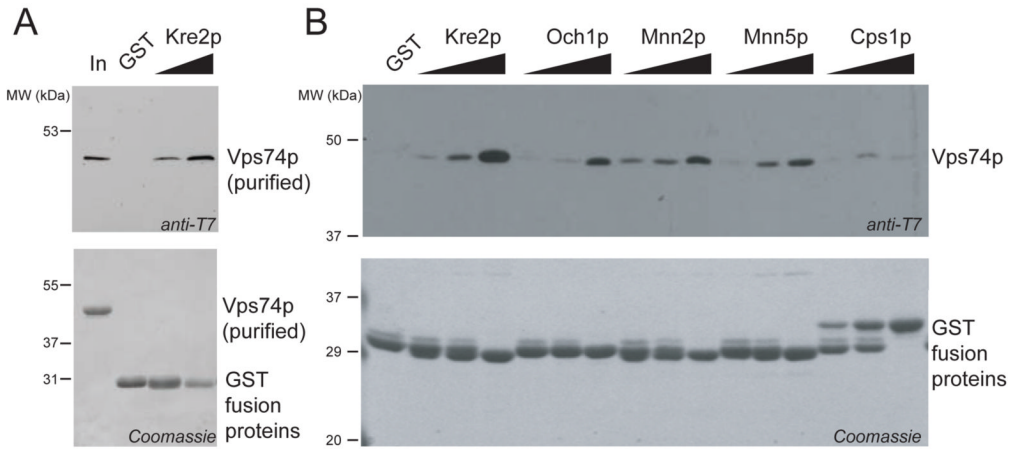

Figure 3. Vps74p binds to the cytosolic domains of Golgi mannosyltransferases

(A) Fusion protein consisting of the first 15 amino acids of Kre2p followed by GST was immobilized on GSH beads. Beads were resuspended in binding buffer (PBS plus 5 mM $MgCl_2$, 1 mM DTT, 0.1% Triton X-100), and incubated with purified T7-epitope-tagged Vps74p. A constant total amount of bait protein was used, with ratios of GST-fusion:GST of 1:1 and 1:0. After incubation the beads were washed five times and bound proteins eluted by denaturation. The top panel shows an anti-T7 immunoblot to visualize bound Vps74p and the bottom panel shows a Coomassie stained gel of the immobilized proteins. The lane labeled "In" in the upper panel (anti-T7 blot) contains 0.5 % of input, and in the lower panel (Coomassie) contains 1 μg of purified T7-Vps74p. The migration of molecular mass standards (kDa) is indicated.

(B) Fusion proteins consisting of the first 15 amino acids of the indicated yeast protein followed by GST were immobilized on GSH beads. Beads were resuspended in binding buffer and incubated with *E. coli* extract containing T7 epitope-tagged Vps74p. A constant amount of bait protein was used in GST-fusion:GST ratios of 1:5, 1:1, 1:0. The amount of Vps74p protein bound to the GST-fusion proteins under these conditions is sub-stoichiometric, suggesting that the binding affinity is relatively weak in this assay.

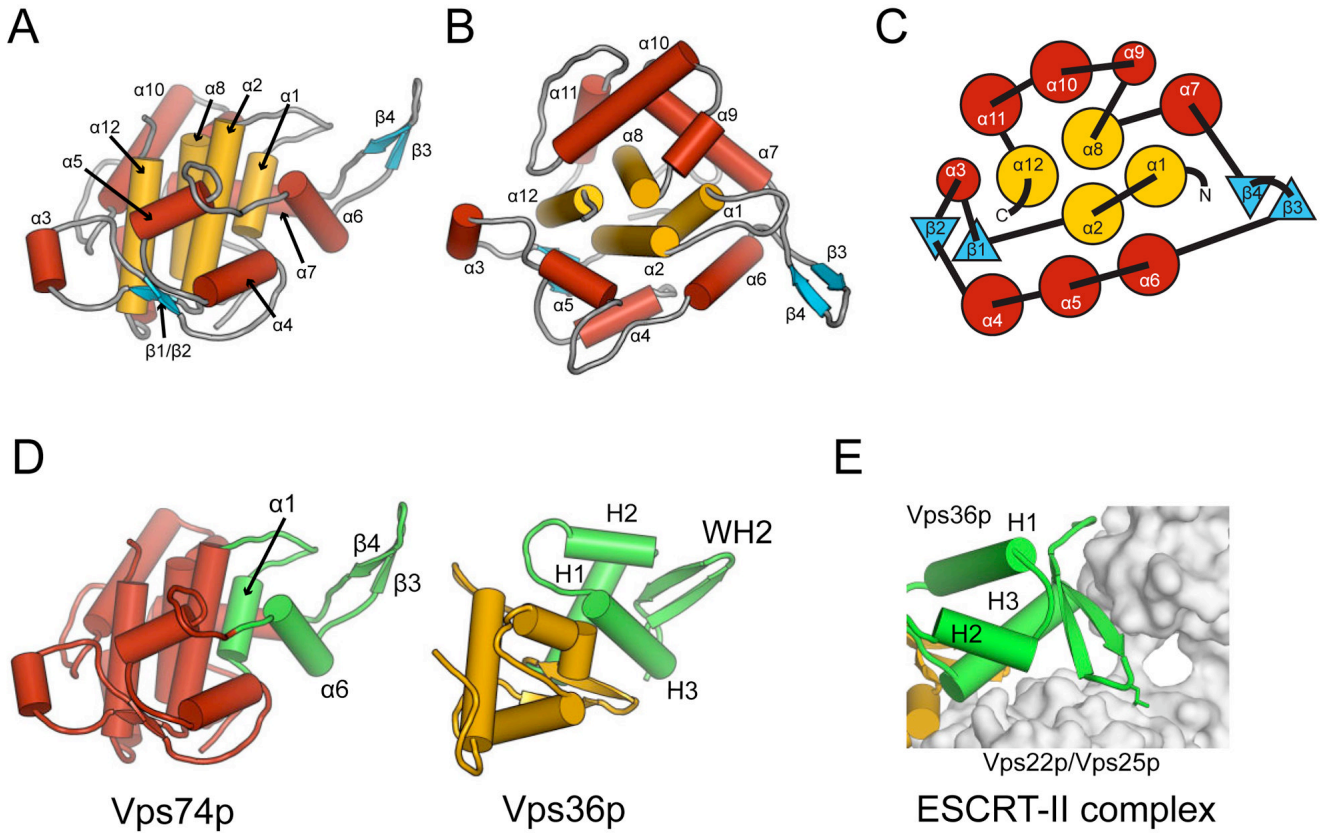

Figure 4. Vps74p has a novel structure that shares features with the proteins of the ESCRT-II complex

(A) Cartoon of Vps74p. Four α-helices (gold) form a central core, encased by loops (gray) and amphipathic α-helices (red). A prominent feature of the structure is a hairpin, formed by β-strands 3 and 4, that projects away from the helical domain.

(B) A view looking down the central α-helical bundle, an approximate 90° rotation about a horizontal axis with respect to A.

(C) A representation of the topology of Vps74p using the same colors as in A.

(D) The β-hairpin region (green) of Vps74p (left hand cartoon) shares structural features with the winged helix (WH) motif, here represented by the second WH domain of Vps36p (green in the right hand cartoon; pdb id 1U5T). The α6 helix and β3/β4 hairpin of Vps74p correspond to the helix H3 and the β-hairpin/wing region of the WH fold. In Vps74p the helical base is extended by helix α1, which occupies the same position as the H1 helix in the WH fold.

(E) The β-hairpin region of the WH2 domain of Vps36p (green) projects into a binding pocket at the center of the ESCRT II complex. A molecular surface is drawn around the other three proteins of this complex (from pdb id 1U5T). In this view Vps36p has been rotated approximately 90° about a horizontal axis with respect to the orientation in D (same orientation as B).

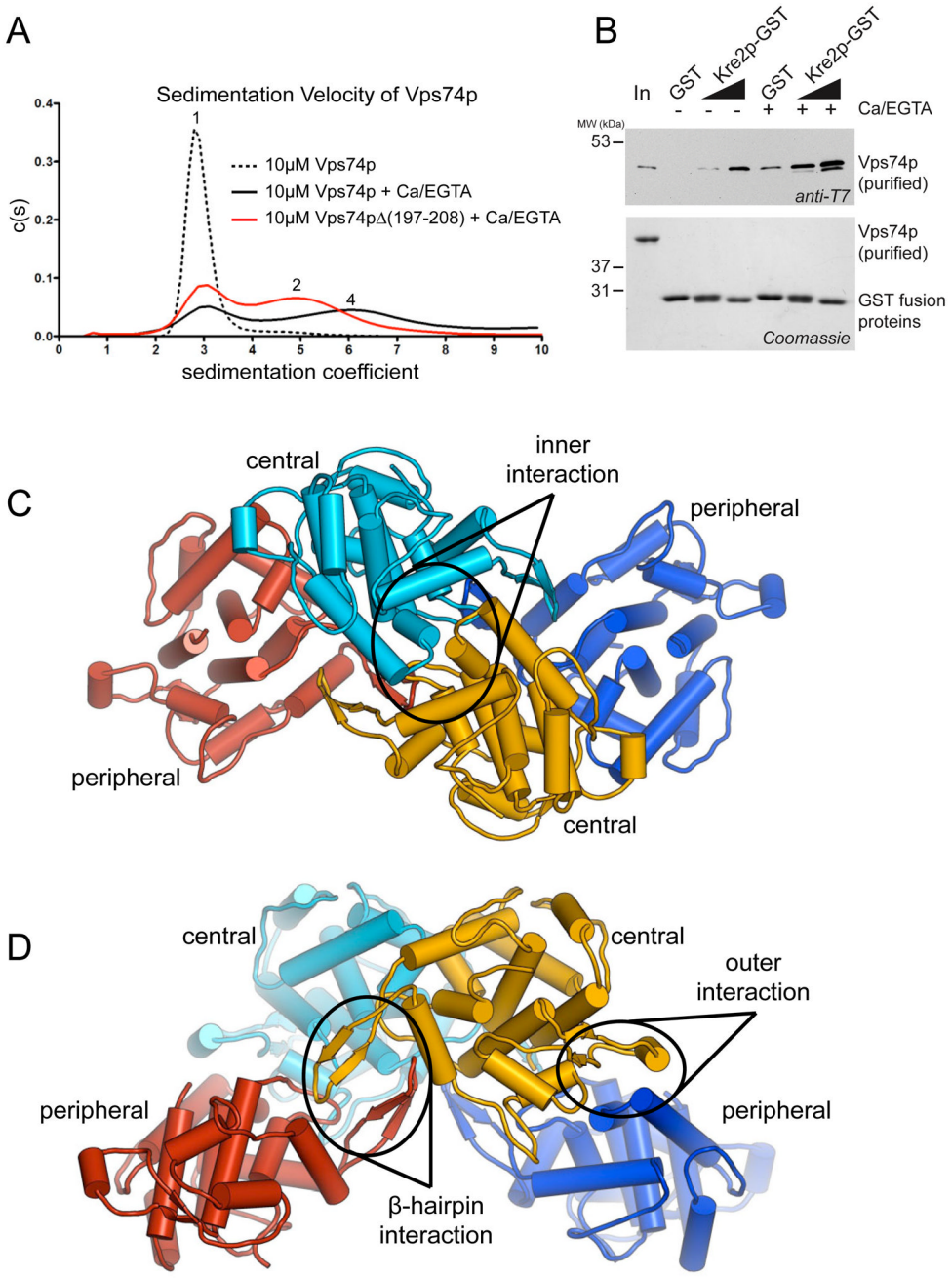

Figure 5. Vps74p forms a tetramer in solution and in the crystal

(A) Sedimentation velocity analytical ultracentrifugation analysis of Vps74p by sedimentation coefficient distribution, *c(s)*. All experiments were conducted with 10 μM protein in 20 mM HEPES, 150 mM NaCl, pH 7.5. The dashed black line represents the species distribution of full- length Vps74p. The solid black line represents full-length Vps74p plus 10 mM $CaCl_2$ and 10 mM EGTA. The red line represents Vps74pΔ (197–208) plus 10 mM $CaCl_2$ and 10 mM EGTA. Numbers indicate the order of the oligomeric species (monomer, dimer, or tetramer) that corresponds to the observed peak.

(B) The interaction of purified T7-tagged Vps74p with immobilized Kre2p-GST was compared in binding buffer, and in binding buffer supplemented with 10 mM $CaCl_2$ and 10 mM EGTA.

Binding assays were performed as for Fig. 3A. A modest enhancement in the amount of bound Vps74p is observed in the presence of Ca/EGTA.
(C) Vps74p forms a two-fold symmetric tetramer structure, shown in cartoon representation, comprising two central subunits (cyan and gold) and two peripheral subunits (red and blue).
(D) In this view, an approximate 90° rotation about a horizontal axis with respect to B, the interfaces between the two peripheral subunits and the gold central subunit can be seen. The β-hairpin of the red peripheral subunit makes extensive interactions with the β-hairpin of the central (gold) subunit. This central (gold) subunit also makes a less extensive outer interaction with the blue peripheral subunit.

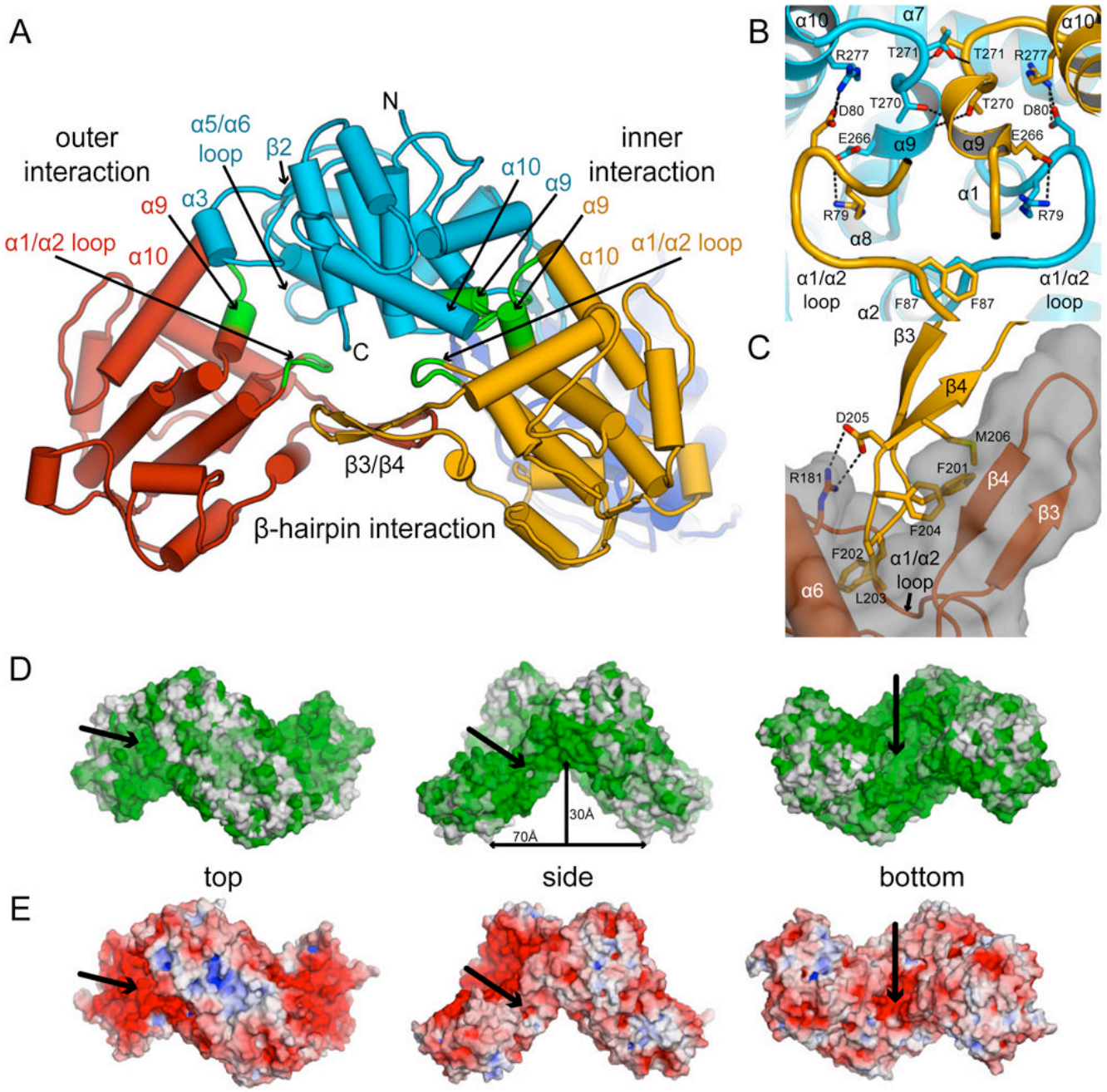

Figure 6. Features of the Vps74p tetramer

(A**)** In this view the approximate two fold symmetry of the β-hairpin interaction can be seen. Structural elements that contribute to the three protein interfaces are labeled. In each of the three subunits that are clearly shown in this view, the α1-α2 loop, helix α9 and the α9-α10 loop are highlighted in green. See text for details.

(B**)** Detailed view of the central interaction. Side chains that make contacts across the interface are shown in stick representation. Hydrogen bond/salt bridge interactions are shown with dashed lines.

(C) Close up view of the interaction of the tip of the β-hairpin with the pocket formed by helix α6 and the α1/α2 loop. The side chains at the tip of the β-hairpin from the gold subunit (amino

acids 202–206) are shown in stick representation. A transparent surface is shown around the red subunit.

(D) A surface representation of the tetramer is shown in three orthogonal views. The surface is colored in a gradient from dark green to white according to the degree of sequence conservation of the surface exposed amino acids among fungal Vps74p proteins (Fig. S2), with dark green indicating the highest sequence conservation. The top and side views are in the same orientations as in Fig 5C and D, respectively.

(E) The electrostatic potential from −8 kT (red) to +8 kT (blue) is projected on to the same surface representations of the Vps74p tetramer. Electrostatic potential calculations used the Adaptive Poisson-Boltzmann Solver (APBS) implemented in Pymol (Baker et al., 2001; DeLano, 2004). Charged side chains not visualized in electron density maps were added using the program CNS (Brunger et al., 1998). Arrows in D and E indicate noted sites of strong sequence conservation and/or electronegativity.

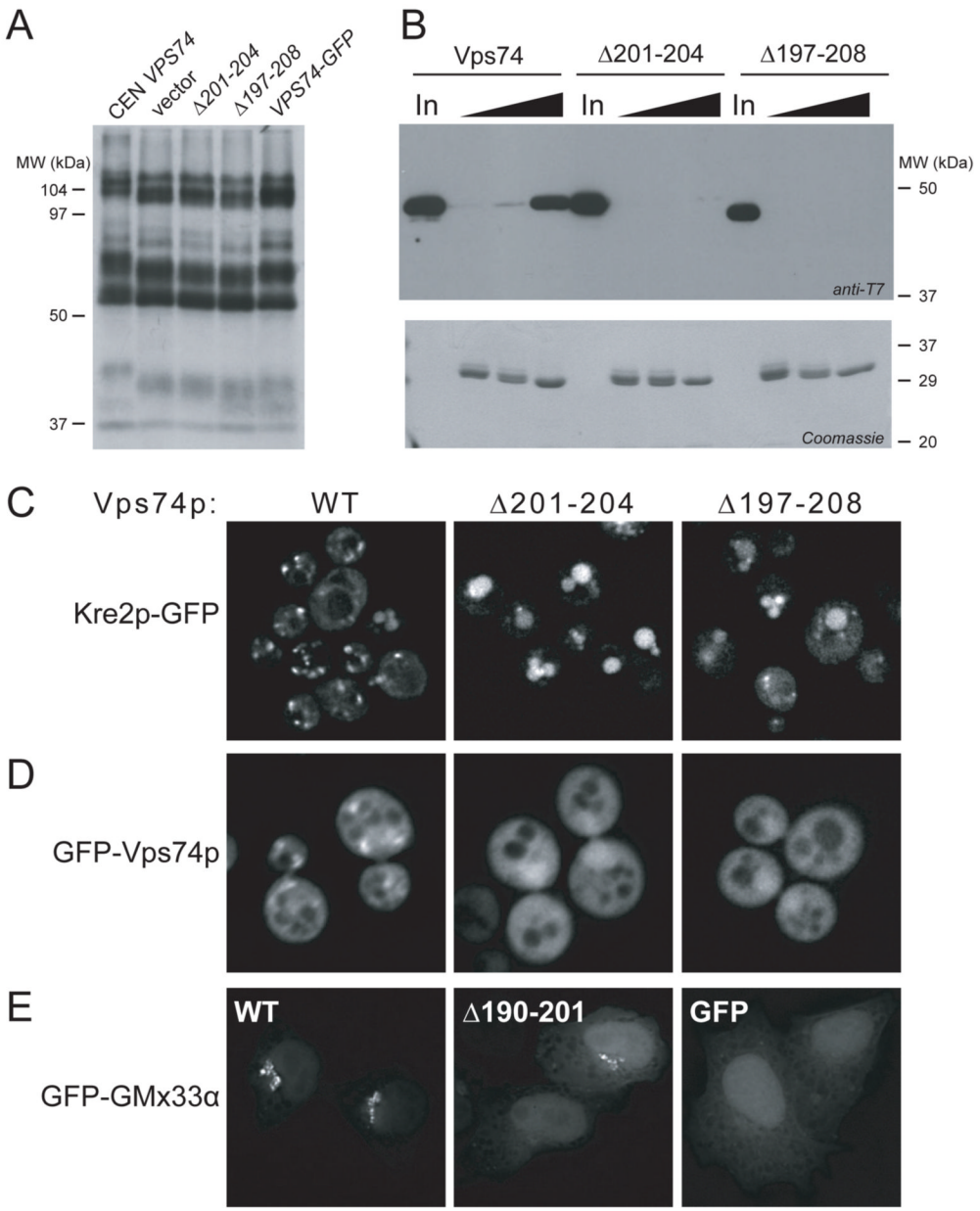

Figure 7. Alterations that disrupt tetramer formation also affect Vps74p function

(A) Pulse-chase analysis of secreted proteins. A *vps74*Δ strain was transformed with single copy vectors encoding wild-type Vps74p (CEN *VPS74*), empty vector, or altered forms of Vps74p and pulse-chase assays were performed as described for Fig. 1A. The right lane (VPS74-GFP) shows the analysis of a strain that expresses Vps74p with a C-terminal GFP-tag expressed from the *VPS74* locus.

(B) Binding of wild-type and the indicated altered forms of Vps74p to the Kre2p-GST fusion protein. Assays were performed as described for Fig. 3. The lanes labeled “In” contain approximately 1% of input material.

(C) Kre2p-GFP localization in *vps74*Δ mutant cells. A *vps74*Δ strain expressing Kre2p-GFP from its native locus was transformed with a single copy vector encoding wild-type Vps74p

(WT) or the indicated altered forms of Vps74p. Fluorescence microscopy was used to visualize Kre2p-GFP. One plane of the deconvolved Z-axis stack is shown.
(D) β-hairpin deletion variants of Vps74p do not localize to the Golgi apparatus. A *vps74*Δ strain was transformed with single copy vectors that express N-terminal GFP-fusions of wild-type Vps74p (WT), or the indicated altered forms of Vps74p. Cells were visualized by fluorescence microscopy. One plane of the deconvolved Z-axis stack is shown.
(E) Micrographs of transfected HeLa cells expressing human wild-type GFP-GMx33α, GFP-GMx33α (190–201), that lacks the region homologous to the Vps74p β-hairpin, or GFP alone. One plane of the deconvolved Z-axis stack is shown. Anti-GFP blotting of cell extracts indicated that GFP-GMx33α and GFP-GMx33α (190–201) were present in roughly equal amounts.

Table 1

Data collection and refinement statistics.

	Vps74p (native)	SeMet-Vps74p (peak)[a]	SeMet-Vps74p (inflection)[a]	SeMet-Vps74p (remote)[a]	Vps74pΔ59
Data Collection Statistics[b]					
Space group	$P3_121$	$P3_121$	$P3_121$	$P3_121$	$P3_121$
Unique cell dimensions	a, b = 102.7 Å, c = 292.3 Å	a, b = 101.5 Å, c = 293.1 Å	a, b = 101.9 Å, c = 293.7 Å	a, b = 101.4 Å, c = 290.8 Å	a, b = 104.1 Å, c = 292.8 Å
X-ray source	APS 23-ID-D	APS 23-ID-D	APS 23-ID-D	APS 23-ID-D	CHESS F1
Wavelength	1.03602 Å	0.97926 Å	0.97942 Å	0.94927 Å	0.918 Å
Resolution limit	2.8 Å	3.4 Å	3.55 Å	2.9 Å	3.05 Å
Observed/Unique	228,024/43,558	254,363/24,850	214,868/21,767	388,891/38,973	218,302/35,872
Redundancy	5.2 fold	10.2 fold	9.9 fold	10.0 fold	6.1 fold
Completeness (%)	97.4 (83.8)	99.0 (95.4)	98.6 (91.8)	98.9 (89.6)	99.8 (100)
R_{sym}[c]	0.093 (0.342)	0.140 (0.456)	0.141 (0.584)	0.116 (0.459)	0.142 (0.529)
$\langle I/\sigma \rangle$	23.7 (2.9)	21.3 (3.3)	18.1 (2.3)	26.2 (2.6)	14.9 (3.25)
Refinement Statistics					
Resolution limits	38-2.8 Å				49-3.05 Å
# reflections/# test set	41,312/2,087				34,003/1,700
R factor (R_{free})[d]	0.24 (0.30)				0.22 (0.28)
Model					
Protein	4 × Vps74p				4× Vps74pΔ59
	aa 61-343[e]				aa 61-343[e]
	5 water molecules				2 water molecules
Total number of atoms	9,079				9,068
RMSD bond lengths (Å)	0.013				0.013
RMSD bond angles (°)	1.499				1.651

[a] SeMet-Vps74p peak and remote datasets were collected on the same crystal; inflection was collected on a second crystal.

[b] Numbers in parenthesis refer to last resolution shell.

[c] $R_{sym} = \Sigma|I_h - \langle I_h \rangle| / \Sigma I_h$, where $\langle I_h \rangle$ = average intensity over symmetry equivalent measurements.

[d] R factor = $\Sigma|F_O-F_C|/\Sigma F_O$, where summation is over data used in the refinement; R_{free} includes only 5% of the data excluded from the refinement.

[e] Number of missing amino acids varies by chain.